Exploring the potential of nitride and carbonitride MAX phases: Synthesis, magnetic and electrical transport properties of V_2GeC, $V_2GeC_{0.5}N_{0.5}$, and V_2GeN

*Niels Kubitza[a], Benedikt Beckmann[b], Sanja Jankovic[a], Konstantin Skokov[b], Aysha A. Riaz[c], Christoph Schlueter[d], Anna Regoutz[c], Oliver Gutfleisch[b], and *Christina S. Birkel[a,e]*

[a]Department of Chemistry and Biochemistry, Technical University of Darmstadt, 64287 Darmstadt, Germany

[b]Institute of Materials Science, Technical University of Darmstadt, 64287 Darmstadt, Germany

[c]Department of Chemistry, University College London, 20 Gordon Street, London WC1H 0AJ, United Kingdom.

[d]Deutsches Elektronen-Synchrotron DESY, 22607 Hamburg, Germany.

[e]School of Molecular Sciences, Arizona State University, Tempe AZ-85282, USA.

Email: Christina.Birkel@asu.edu

ABSTRACT

The chemical composition variety of MAX phases is rapidly evolving in many different directions, especially with the synthesis of carbides that contain two or more metals on the *M*-site of these layered solids. However, nitride and carbonitride MAX phases are still underrepresented and only a few members have been reported, that are for the most part barely characterized, particularly in terms of magnetic and electronic properties. Here, we demonstrate a simple and effective synthesis route, as well as a comprehensive characterization of three MAX phases, (i) V_2GeC, (ii) the hitherto unknown carbonitride $V_2GeC_{0.5}N_{0.5}$, and (iii) the almost unexplored nitride V_2GeN. By combining a microwave-assisted precursor synthesis with conventional heat treatment and densification by spark plasma sintering, almost phase pure (carbo)nitride products are obtained. Magnetic measurements reveal an antiferromagnetic-paramagnetic-like phase transition for all samples in the temperature range of 160 K - 200 K. In addition, increasing the amount of nitrogen on the *X*-site of the MAX phase structure leads to a constant increase of the magnetic susceptibilities while the electrical resistivity is constantly decreasing. Overall, these findings provide crucial insights how to tune electronic and magnetic properties of MAX phases by only varying the chemical composition of the *X*-site. This further substantiates the demand for (carbo)nitride research with the potential to be extended to the remaining elemental sites within the MAX phase structure in order to push towards controlled material design and to achieve desired functional properties, such as ferromagnetism.

INTRODUCTION

MAX phases, a unique class of hexagonally layered ternary transition metal carbides and (carbo)nitrides have experienced a significant boost in research activities over the recent years. While the first solely synthesis driven reports of these types of materials reach back to the 1960s,[1–5] Barsoum *et al.* discovered their ability to combine metallic and ceramic properties with the synthesis of Ti_3SiC_2 in the late 1990s.[6] A few years later in 2000, the name ”MAX phases” was coined along with a first comprehensive review summarizing roughly 50 members and their characteristics.[7] Since then, the general formula is expressed as $M_{n+1}AX_n$ (n = 1, 2, 3 (4,5)), where M is an early transition metal, A is a main group element mostly of groups 13 and 14, and X is carbon and/or nitrogen. The crystal structure can be described by edge-shared M_6X octahedra interleaved with layers of A elements, resulting in the space group $P6_3/mmc$.[8] After the year 2000, an almost exponential increase in the phase (chemical composition) variety can be observed, ranging from the discovery of new solid-solution phases,[9–12] such as ordered MAX phases,[13,14] towards compositionally complex compounds,[15–17] leading to more than 340 reported members until now.[18,19] This number has just very recently been tremendously affected by the group of Huang,[20] reporting a new approach to use chemical scissors to specifically replace the A-elements by uncommon elements, such as iron or zinc. As a consequence of the development in recent years, the property profile has been broadened, now including superconductivity, [21–23] the role as MXene precursors,[17,24,25] or complex magnetic behavior.[26–29]

However, most of these novelties and reports concentrate only on carbide MAX phases, whereas nitrides and carbonitrides are significantly underrepresented. For instance, in the very recent comprehensive review by Dahlqvist *et al.* in 2023, summarizing the hitherto reported MAX phase in numbers,[18] only about 7 % of all members contain nitrogen on the X-site. Furthermore, for most

of the known nitrides, the reports only include the pioneering work of the 1960s and thus no information beyond their synthesis parameters, if provided at all.[2,30,31] Reasons for these vast differences can be attributed to challenges occurring in the nitride synthesis, such as the gaseous state of nitrogen under normal conditions, or its high bonding energy.[32] Additionally, contrary to carbides, binary nitride precursors are required to maintain MAX phase stoichiometry, resulting in an additional synthesis step and an additional degree of complexity.[33] Nonetheless, besides these challenges, nitrides have already proven to exhibit advantages over their carbide counterparts, as shown with higher electronic conductivities (Ti_2AlN[34]) or enhanced magnetic correlations (Cr_2GaN[35,36]). The latter example, showing a spin density wave state at T = 170 K[35], impressively demonstrates the potential of nitrides in contrast to carbides and is to the best of our knowledge the only magnetic study of conventionally synthesized MAX phase nitrides to date, whereas carbonitrides have not been magnetically investigated at all yet. With regard to magnetism, most efforts have been directed towards the synthesis of new *M*-site Mn-doped Cr_2AC (A = Al, Ga, Ge) phases[4,22,23,37–39] , while recent studies also focus on the incorporation of ferromagnetic elements on the *A*-site of MAX phases.[40,41]

For the here described V-Ge-C-N system, these imbalances between carbide and nitride studies also apply. While several reports of the synthesis and properties of the carbide V_2GeC exist,[42–45] there is only one published short communication paper on the nitride V_2GeN (1960s)[2] in which its discovery was reported, however, without any experimental information or profound characterization data, such as unit cell parameters. Therefore, this MAX phase has not been listed in recent review articles.[8,18] On the other hand, the respective carbonitrides are hitherto entirely unknown. This is reminiscent of the Ga-based counterpart system V_2GaC/N, where until last year only the carbide had been described in more detail.[33] While in the latter project, our group focused

on the development of a new wet-chemical assisted synthesis approach, this time, we focus on the characterization of the properties by accurately adjusting the chemical composition. Therefore, we applied a combination of a microwave-assisted precursor synthesis, followed by a conventional heat treatment and densification by spark plasma sintering to achieve high-quality samples. The three target materials are (micro)structurally and chemically characterized by means of X-ray powder diffraction (XRD), hard X-ray photoelectron spectroscopy (HAXPES), and electron microscopy (SEM), and magnetometry and resistivity measurements are used to discuss their functional properties.

EXPERIMENTAL

Step 1: Vanadium nitride precursor synthesis:

In order to prevent oxygen impurities during the weighing process, the following steps were performed inside an Ar-filled glovebox. According to Vaidhyanathan *et al.*[46], 1 g (15.4 mmol) vanadium powder (Alfa Aesar, ~325 mesh, 99.5 %) and 1 g (18.7 mmol) NH_4Cl (technical) were finely ground using an agate mortar. Afterwards the reactant mixture was pressed into a dense pellet (⌀= 10 mm, 5 t, 30 s) and transferred into a fused silica ampoule, equipped with a custom-made vacuum adapter. Subsequently, the sample was transferred into a microwave oven (CEM Microwave Technology Ltd., MARS 6) and flushed for 10 minutes with flowing nitrogen before commencing heat treatment (800 W, 30 min, 7 g carbon (Gruessing, granules, 2.5 mm) as susceptor material) under continuous nitrogen flow. Prior to characterization, the pellets are finely ground and stored under atmospheric conditions.

Step 2: MAX phase synthesis:

The V_2GeC phase was prepared by using exclusively elemental precursors, while VN (step 1) was used for the synthesis of V_2GeN and the carbonitride $V_2GeC_{0.5}N_{0.5}$, according to the following reaction equations (1-3):

$$2\,V + Ge + C \rightarrow V_2GeC \quad (1)$$

$$1.5\,V + 0.5\,VN + 1\,Ge\ + 0.5\,C\ \rightarrow V_2GeC_{0.5}N_{0.5} \quad (2)$$

$$1\,V + 1\,VN + 1\,Ge\ \rightarrow V_2GeN \quad (3)$$

All precursor amounts were based on producing two pellets of 0.5 g each of the desired MAX phase. A detailed summary can be found in the SI (**Table SI-1**). Inside the glovebox, germanium (99.999 %, Thermoscientific) was mixed with the remaining reactants vanadium (Alfa Aesar, ~325 mesh, 99.5 %), vanadium nitride (step 1), and graphite (Alfa Aesar >99.9 %, APS 2-15 µm) according to the aforementioned reactions and pressed into a dense pellet (⌀= 10 mm, 5 t, 30 s). Afterwards, the pellets were transferred into fused silica ampoules and heat treated in a chamber furnace (Snoltherm) following a defined temperature program (**Table SI-2**). Prior to characterization of the samples by means of XRD, SEM and HAXPES, the pellets were finely ground using an agate mortar. Please note that we refer to the carbonitride using the nominal sum formula $V_2GeC_{0.5}N_{0.5}$.

For further characterization, 0.85 g of the sample material were densified using spark plasma sintering (Dr. SinterLab SPS-211Lx, Fuji). Here, the powders were transferred into a graphite die

(⌀= 10 mm), equipped with two graphite stamps and graphite foil to separate the powder from the die wall and stamps. During the pressing process, the reaction chamber was evacuated, and the initial pressure was set to 30 MPa at room temperature, before the temperature was increased to 600 °C. Subsequently, the pressure was set to 100 MPa before the temperature was further increased to 1000 °C, which was held for 15 minutes. A representative temperature and pressure profile can be found in **Figure SI-1**. The samples were cooled to room temperature, before the pressure was released. Remaining graphite residues were removed by polishing the pellets on a diamond plate. The degree of compaction was determined using gas pycnometer AccuPyc 1340 (Micromeritics GmbH) measurements.

Characterization:

XRD data were obtained using a Stadi P (Stoe & Cie GmbH) with monochromatized Cu-$K\alpha_1$ radiation (λ = 1.540596 Å) and a Mythen 1K (Dectris) detector in transmission geometry at room temperature. For measurements, small sample amounts were deposited between X-ray amorphous adhesive film (Scotch) on a flat sample holder and rotated orthogonally to the X-ray source. Rietveld refinements were performed using the program TOPAS (Version 4.2, Bruker). For lattice parameter determination, LaB_6 (NIST, 660c)[47] standard measurements were performed. Side phase amounts in weight-% were determined based on the structural model of V_2GeC afterwards,[48] before the extracted lattice parameters were used for Le Bail fitting of the X-ray diffraction data.

SEM images were taken using a XL30 FEG (Philips) with an acceleration voltage of 25 kV adapted with an APOLLO X-SDD detector (EDAX) for collecting energy dispersive X-ray spectroscopy (EDX) data. The EDX data was evaluated using the software EDAX GENESIS. The SPS densified samples were imaged using the Vega3 (Tescan) electron microscope.

Hard X-ray photoelectron spectroscopy (HAXPES) was used to characterize the chemical environments and oxidation states of the samples. Data were collected at beamline P22 at PETRAIII, German Electron Synchrotron DESY in Hamburg, Germany.[49] A photon energy of 6 keV was used for all experiments, with the energy selected using a Si (111) double-crystal monochromator. A Phoibos 225HV analyzer (SPECS, Berlin, Germany) was used with the small area lens mode and a slit size of 3 mm. Spectra were collected at room temperature using a pass energy of 30 eV. The total energy resolution in this setup was determined to be 245 meV 16/84% Fermi edge (E_F) width of a polycrystalline gold foil. Samples were mounted using conducting carbon tape.

Magnetic measurements were performed with a magnetic property measurement system MPMS-3 (Quantum Design). Isofield measurements were carried out with a continuous heating and cooling rate of 2 $Kmin^{-1}$. Isothermal measurements were performed by stabilizing the magnetic field at each measurement point. To avoid non-linearities in the magnetization signal at low magnetic fields, the magnetic susceptibility χ was calculated from the difference of the isofield magnetization curves measured in magnetic fields of 5 and 7 T, such that $\chi(T) = (M(T)_{7T} - M(T)_{5T})/2T$. Complementary, the susceptibility was determined from the linear regression of the isothermal magnetization curves in the field range from 5 to 7 T. In addition, the temperature-dependence of the susceptibility in alternating magnetic fields χ_{AC} was measured by stabilizing the temperature at each measurement point, using an alternating field of 0.001 T with a frequency of 10 s^{-1}.

The electrical resistivity was measured with a two-electrode setup implemented in a physical property measurement system PPMS-14T (Quantum Design). A detailed description of the measurement setup can be found elsewhere.[50]

RESULTS AND DISCUSSION

Structural Analysis

Starting from the elemental precursors to synthesize the carbide phase V_2GeC, the amount of nitrogen was nominally increased twice (50 at-% each) by adding vanadium nitride according to the chemical equations (1-3) shown above. The highly crystalline VN precursor material was obtained single phase and the extracted lattice parameters fit well to those reported in literature (**Figure SI-2, Table SI-3**).[51] The same sample quality is observed for the parent carbide phase V_2GeC as shown by the refined XRD data in **Figure 1**. No additional side phases are detected and the lattice parameters fit well to those initially reported by Jeitschko *et al*.,[5] as well as to experimental values of more recent work by Phatak *et al*.[52] Both the carbonitride and nitride samples show small amounts of vanadium nitride and elemental germanium as assignable side phases, however, in total only less than 6 wt-% each are found, substantiating a good sample quality (**Table SI-4**). For detailed extraction and comparison of the lattice parameters of all three target materials, LaB_6 standard measurements were performed (**Figure SI-2**, **Table SI-5**). The determined lattice parameters were then used for a subsequent Le Bail refinement (**Figure 1, Table 1)** using the structural model of V_2GeC[52] providing the space group $P6_3/mmc$. By increasing the nitrogen amount towards 50 at-%, a small elongation in the *c*-direction is observed, while the *a*-lattice parameter slightly decreases. Overall, this results in a shrinkage of the cell volume by ~0.4 $Å^3$. Similar behavior applies to the pure nitride phase. However, here, the *c*-lattice parameter

increases slightly more significantly than for the carbonitride, and the decrease of the *a*-lattice parameter is also slightly more pronounced (**Figure 1**).

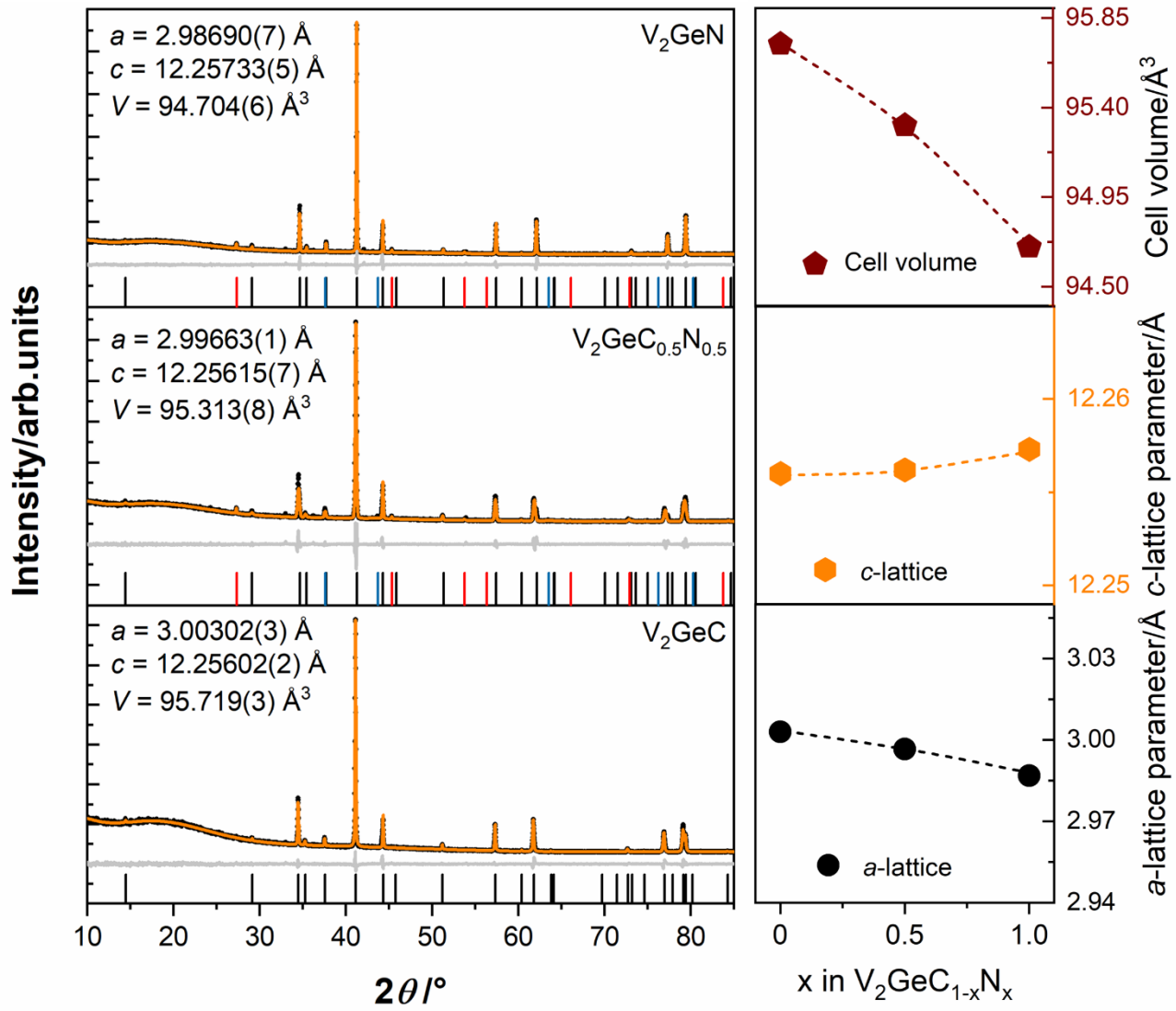

Figure 1: Le Bail refinements (orange lines) of the XRD data (black dots) of V_2GeC, $V_2GeC_{0.5}N_{0.5}$, V_2GeN, based on the structural model of V_2GeC[52] providing the space group $P6_3/mmc$. The lattice parameters were determined beforehand by standard LaB_6 measurements (SI). Red markers represent germanium[54] peak positions and blue markers vanadium nitride[51] peak positions. Besides, the lattice parameters (*a,c*), as well as the cell volumes of the respective phases are plotted against the nominal nitrogen amount. The dashed lines are drawn for guidance.

This leads to a further shrinkage of the cell volume of ~0.6 $Å^3$ which is overall consistent with the smaller atomic radius of nitrogen (1.79 Å) compared to carbon (1.90 Å).[53] In comparison, the structural parameters of the carbonitride sit in between the two parent phases which confirms the nominal composition of $V_2GeC_{0.5}N_{0.5}$. Small deviations of an exact linear trend can also occur due

to instrumentation inaccuracies, since the investigated 2θ range is extremely small (e.g., *c*-lattice parameter ~0.001 Å). In comparison to the 211 V-Ga-C-N system, a similar evolution of the lattice parameters from carbide to nitride was observed which further supports the obtained structural results.[33]

Table 1: Summary of the Le Bail refinements of V_2GeC, $V_2GeC_{0.5}N_{0.5}$ and V_2GeN based on the structural model of V_2GeC providing the space group $P6_3/mmc$.[52]

Phase name	V_2GeC (lit)[52]	V_2GeC	$V_2GeC_{0.5}N_{0.5}$	V_2GeN
Lattice parameters/Å	a = 3.001 c = 12.2601	a = 3.00302(3) c =12.25602(2)	a =2.99663(1) c =12.25615(7)	a = 2.98690(7) c =12.25733(5)
Cell volume/Å^3	95.36	95.719(3)	95.313(8)	94.704(6)
Background order		15	15	15
R_p		3.08	5.13	4.07
R_{wp}		4.74	8.57	7.18
R_{exp}		2.55	3.25	2.76
GOF		1.86	2.64	2.60

The morphology of the target materials is investigated using SEM. As shown in **Figure 2a-c**, all samples exhibit MAX phase typical anisotropic layered structures, partially covered with smaller substructures. EDX measurements do not show any anomalies and confirm the 2:1 ratio of V/Ge of the samples. A representative EDX spectrum of V_2GeC is shown in **Figure 2d**. and a comparison between all three phases can be found in **Figure SI-3**. Interestingly, despite significant differences in the respective time for the heat treatments of the materials (10 h, carbide; 30 h, (carbo)nitride) no obvious differences in the morphologies are present. The required increase in

reaction time for the (carbo)nitride can be explained by the involvement of the stable binary nitride precursor vanadium nitride. As a reference, a 10 h heat treatment for the nitrogen containing materials only leads to a phase mixture of the respective MAX phase, germanium, vanadium nitride, and the intermetallic phase Ge_3V_5, as could be shown by ex-situ XRD data (**Figure SI-6**). In addition, this analysis provides further insights into the reaction mechanism: Initially an intermetallic *MA* phase is formed, before the reaction of the *MA* phase with the remaining reactants completes the conversion towards the MAX phase. Similar behavior was reported for the 211 V-Ga-C-N system.[33]

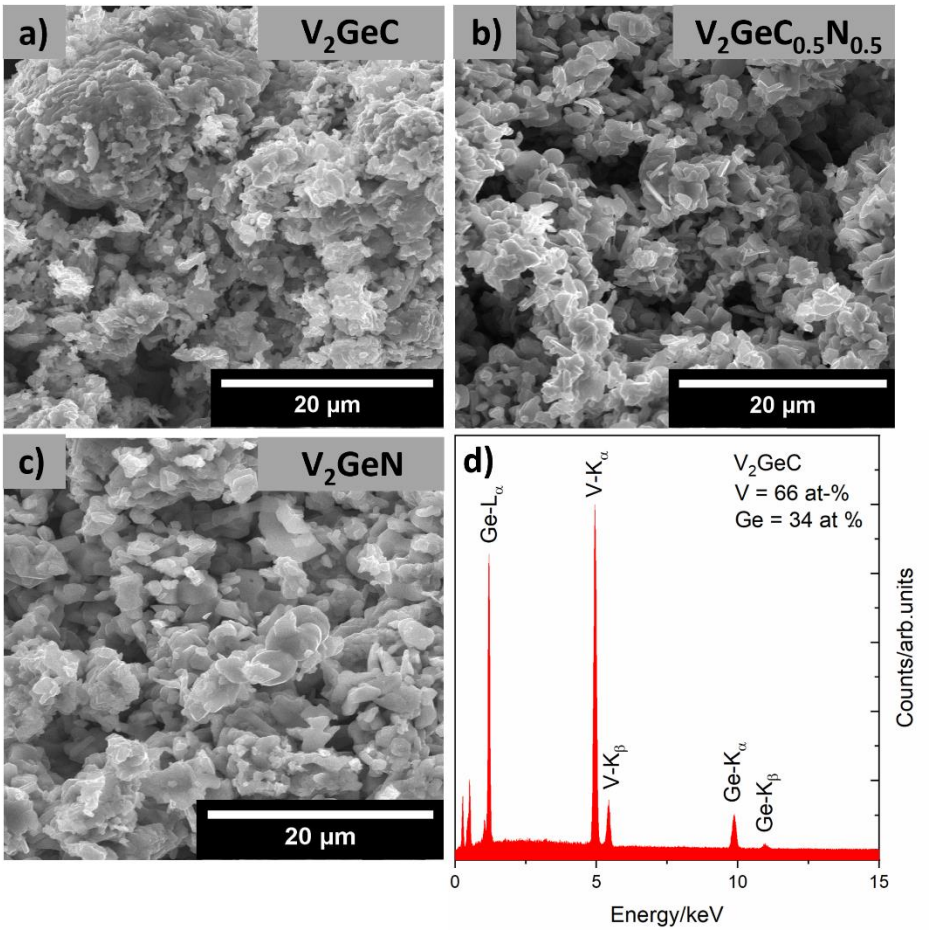

Figure 2: SEM micrographs based on secondary electron (SE) contrast (a-c) showing the morphology of V_2GeC (a), $V_2GeC_{0.5}N_{0.5}$ (b) and V_2GeN (c), respectively. Figure d shows a representative EDX spectrum by the example of V_2GeC.

HAXPES was used to identify the elements and their chemical states present in the three samples, with survey spectra showing all expected lines (**Figure SI-4**). The Ge $2p_{3/2}$ core level (**Figure 3(a)**) shows a main contribution at a binding energy (BE) of 1217.2 eV from GeV_6 environments. In addition, contributions from Ge^{+4} oxide (GeO_2) appear in all samples at a BE of 1220.0 eV. As all samples were handled in air, partial oxidation is expected. The V 2*p* core level spectra (**Figure 3 (b)**) show the typical doublet, with the $2p_{1/2}$ state considerably broadened by Coster-Kronig effects. All samples show clear V-C/N environments with the V $2p_{3/2}$ peak occurring at 512.9 eV. In addition, all samples show contributions from oxidized states at higher BE. Relative to the carbide phase, the carbonitride and nitride phases show a slight reduction in the amount of V present. The C 1*s* spectra (**Figure 3(c)**) clearly distinguish between the pure nitride, and the carbide and carbonitride phases. Only the latter two have a sharplow BE feature at 282.8 eV. All samples exhibit varying contributions from adventitious carbon (C^0) from exposure to air. Finally, the N 1*s* spectra (**Figure 3 (d)**) show one dominant feature at 398.0 eV for the NV_6 environments in the nitride and carbonitride phases. No nitrogen signal is detected in the carbide phase. Additional low intensity shoulders on the higher and lower BE sides of this main peak are ill defined but could arise from vanadium nitride as found from XRD as well as from NH_x and $N_{1-x}C_xV_6$ environments. By comparing the peak intensities of the pure nitride and carbide phases (assuming they are 1:1 Ge:C/N) to those in the carbonitride phase, the C/N ratio is estimated to be 0.56:0.44.

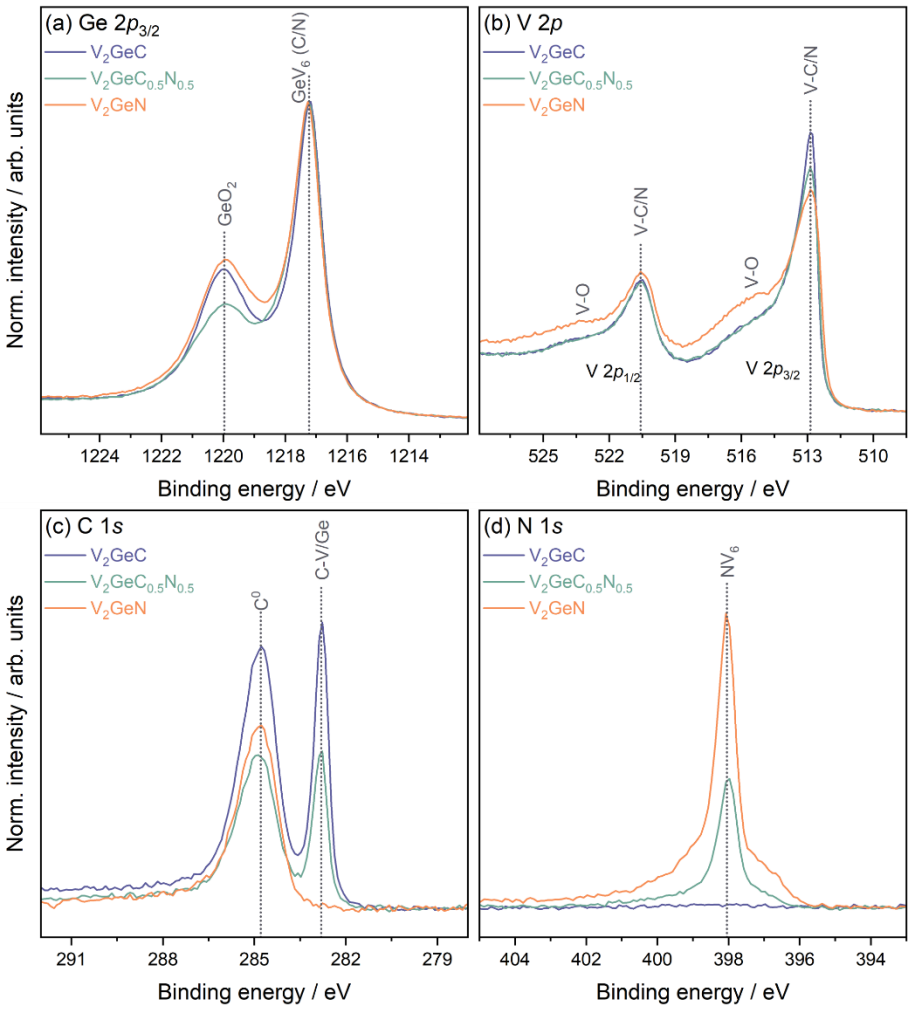

Figure 3: HAXPES core level data of V_2GeC, $V_2GeC_{0.5}N_{0.5}$, and V_2GeN, including (a) Ga $2p_{3/2}$, (b)V $2p$, (c) C $1s$, and (d) N $1s$. All spectra are normalized to the maximum height of their respective Ge $2p_{3/2}$ spectra.

Magnetic and Electronic Analysis

The magnetic properties of V_2GeC, $V_2GeC_{0.5}N_{0.5}$ (nominal) and V_2GeN are shown in **Figure 4** and are summarized in **Table 2**. The isothermal magnetization curves (**Figure 4** (**a-c**)) show distinctively different magnetization behavior for all three MAX phases at 300 and 2 K. At 300 K, all compounds show a strictly linear field-dependent magnetization, typical for paramagnetic MAX phases.[9,29]

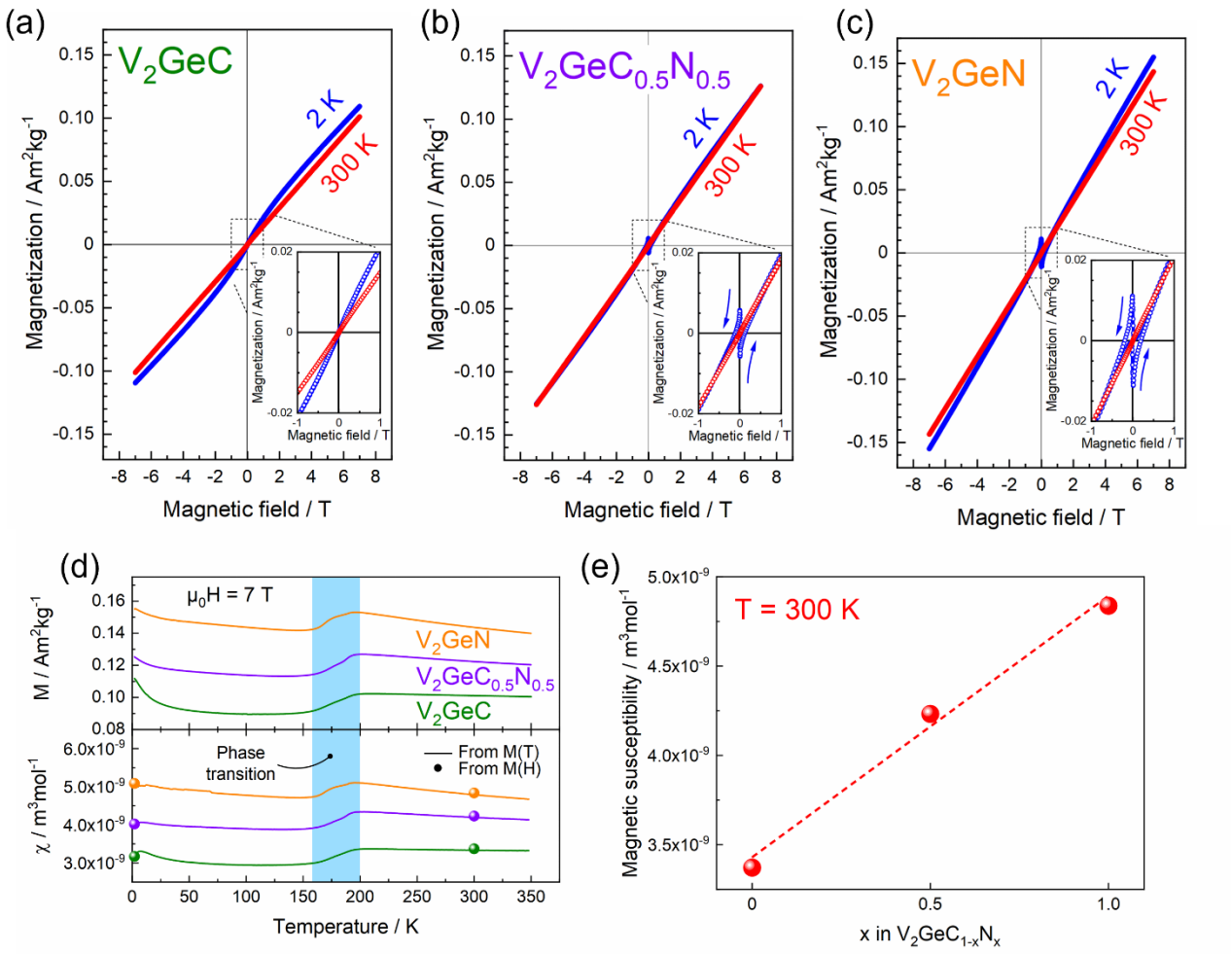

Figure 4: Isothermal magnetization curves at 300 K (red) and 2 K (blue) of (a) V_2GeC, (b) $V_2GeC_{0.5}N_{0.5}$ and (c) V_2GeN. The insets show the curves around zero magnetic field in more detail. (d) Isofield magnetization curves in a magnetic field of 7 T (top panel) and magnetic susceptibility curves (bottom panel) of V_2GeC (green), $V_2GeC_{0.5}N_{0.5}$ (violet) and V_2GeN (orange). The susceptibility has been determined from isofield (solid lines) and isothermal (circles) magnetization measurements. The temperature range showing the phase transition is highlighted. (e) Magnetic susceptibility at 300 K as a function of the nominal nitrogen content in $V_2GeC_{1-x}N_x$ MAX phases. The dashed line is drawn to guide the eye.

However, at 2 K, the magnetization is non-linear with respect to the magnetic field and the hysteresis loops of $V_2GeC_{0.5}N_{0.5}$ and V_2GeN are indicating the presence of a superconducting state. As the dimensionless volume susceptibility is substantially larger than a value of χ = -1 ($V_2GeC_{0.5}N_{0.5}$: $\chi_{2K} = -0.010$, V_2GeN: $\chi_{2K} = -0.017$) the feature in the hysteresis loops does not represent MAX phase bulk superconductivity, but most likely a superconducting secondary

phase, which is not assignable in the XRD data. Based on full hysteresis loops, initial magnetization curves and zero-field χ_{AC} measurements subsequent to zero-field cooling, the superconducting states in V_2GeN (**Figure SI-7**) and $V_2GeC_{0.5}N_{0.5}$ (**Figure SI-8**) show a critical temperature T_c of approximately 6.75 K and 5.25 K, respectively. At this temperature, the in-phase component of the AC-susceptibility χ'_{AC} changes sign from negative to positive values upon heating. The absence of the superconducting state in V_2GeC substantiates its phase purity and the different T_c in $V_2GeC_{0.5}N_{0.5}$ and V_2GeN indicate that its presence and properties can be linked to the nitridation process and the nitrogen content, respectively. The isothermal and isofield magnetization curves as well as magnetic susceptibility curves (**Figure 4** (**d**)) show that the magnetization and susceptibility are increasing with a higher nitrogen content (**Figure 4** (**e**), **Table 2**), indicating an enhanced exchange upon nitridation similar to the 211 Cr-Ga-C-N system.[35] In addition, the temperature-dependence of the magnetization and susceptibility reveal the presence of a phase transition in the investigated $V_2GeC_{1-x}N_x$ MAX phases. For all samples, the transition occurs in the same temperature range from 200 K to 160 K and is accompanied by a similar decrease in magnetization and susceptibility upon cooling, reminiscent of the antiferromagnetic to paramagnetic phase transition in Cr_3GeN.[55,56] However, the exact nature of this transition still has to be elucidated. A magnified representation of the phase transition via the inverse magnetic susceptibility χ^{-1} can be found in **Figure SI-9**. Furthermore, it should be noted that the temperature dependence of the magnetization appears to be tailored by increasing the nitrogen amount in the materials. While the magnetization of the parent carbide phase V_2GeC almost stays constant for temperatures above $T > 200$ K, representing the MAX phase-typical Pauli paramagnetic behavior,[9,35] the carbonitride and even stronger the pure nitride exhibit a noticeable decrease in the magnetization in the same temperature range upon heating. For temperatures below

~40 K, the small increase of the susceptibility is a common feature in MAX phase compounds in general[57] and may be attributed to small paramagnetic impurities. Comparing the most frequent magnetically studied Cr-based MAX phases in literature, such as Cr_2AC(A = Al, Ga, Ge),[35,57,58] the here reported magnetic susceptibility of V_2GeC at 300 K exhibits smaller values. This can be most likely explained due to an increased electron density on the *M*-site[9] and is also consistent for the nitride phase V_2GeN compared with Cr_2GaN.[35] Compared to V_2AlC,[29] V_2GeC exhibits higher susceptibility values.

Table 2: Summary of magnetic and electronic transport properties of V_2GeC, $V_2GeC_{0.5}N_{0.5}$ and V_2GeN MAX phases, including the magnetization at 300 K and 7 T $M_{300K,7T}$, the magnetic susceptibility at 300 K χ_{300K} and the electrical resistivity values at 300 K ρ_{300K} and 10 K ρ_{10K}.

MAX phase	$M_{300K,7T}$	χ_{300K}	χ_{300K}	ρ_{300K}	ρ_{10K}
	Am^2kg^{-1}	m^3mol^{-1}	emu $g^{-1}Oe^{-1}$	μΩm	μΩm
V_2GeC	0.101	$3.4x10^{-9}$	$1.4x10^{-6}$	1.05	0.40
$V_2GeC_{0.5}N_{0.5}$	0.126	$4.2x10^{-9}$	$1.8x10^{-6}$	0.93	0.27
V_2GeN	0.144	$4.8x10^{-9}$	$2.0x10^{-6}$	0.80	0.27

The temperature dependence of the electrical resistivity of V_2GeC, $V_2GeC_{0.5}N_{0.5}$ and V_2GeN is shown in **Figure 5** and is represented in **Table 2** with electrical resistivity values for 300 and 10 K. A metallic behavior can be observed in all three MAX phases as the electrical resistivity decreases upon cooling. This agrees with the substantial electron populations observed at the Fermi energy (E_F) of all three samples in HAXPES valence spectra (**Figure SI-5**). No significant change in electrical resistivity is present at the identified transition around 200 to 160 K (**Figure 4 (d)**), indicating the absence of substantial crystal structure modifications upon the alteration of the magnetic state of the MAX phases, as reported for Cr_2GaN.[36] The *X*-site modification of the

$V_2GeC_{1-x}N_x$ MAX phase, however, allows to substantially tune the electrical resistivity, resulting in an ~25 % increase at 300 K from the nitride phase V_2GeN to the carbide counterpart V_2GeC.

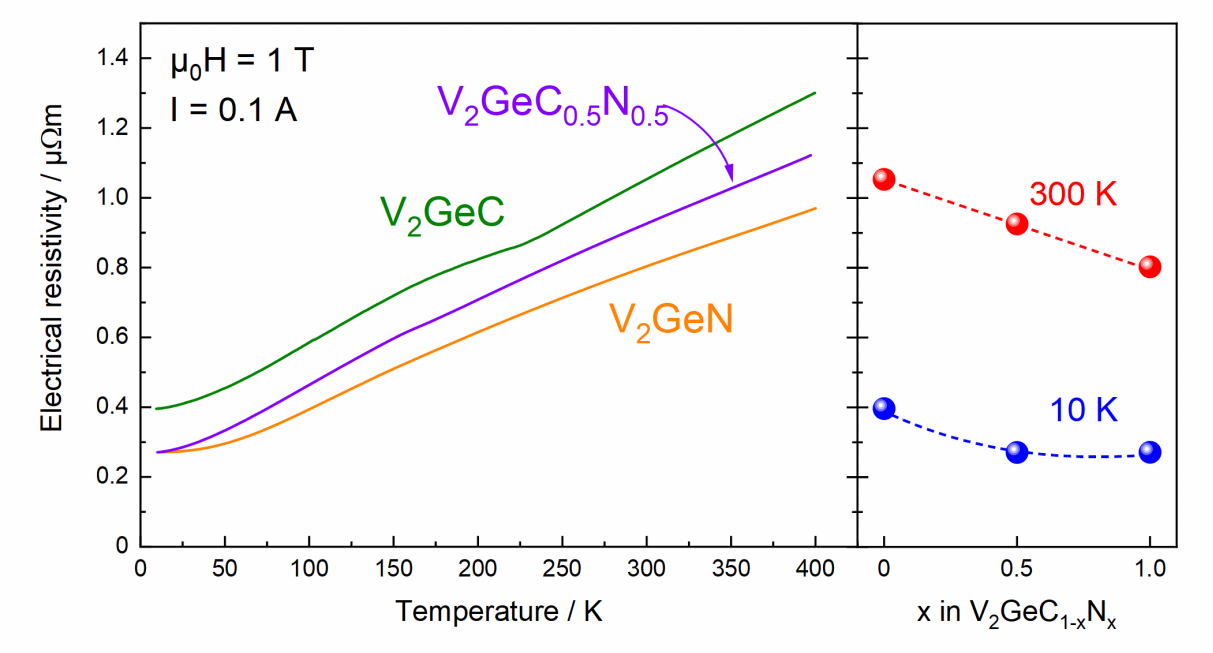

Figure 5: Temperature-dependence of the electrical resistivity (left panel) of V_2GeC (green), $V_2GeC_{0.5}N_{0.5}$ (violet) and V_2GeN (orange), measured in a magnetic field of 1 T and with a current of 0.1 A in the temperature range from 390 K to 10 K. The electrical resistivity at 300 K (red) and 10 K (blue) is also given as a function of the nominal nitrogen content in $V_2GeC_{1-x}N_x$ MAX phases (right panel). Dashed lines are drawn to guide the eye.

Compared to other carbide phases, V_2GeC shows significant higher resistivity values, such as for reactively hot-pressed Nb_2AlC[59] (threefold increase) or Ti_2AlC[34] (fivefold increase). This trend is also confirmed by V_2GeN, which shows an almost fourfold increase in comparison to reactively hot-pressed Ti_2AlN.[34] On the other hand, similar fabricated V_2AlC, using spark plasma sintering for densification, exhibits only differences in the range of 20 %,[29] while the values for reactively hot pressed V_2AlC are almost ten times smaller.[59] Particularly the latter example clearly shows that the measurement of resistivity is highly dependent on the densification technique, due to the strong influence of extrinsic contributions related to microstructural parameters such as particle size, phase purity, and degree of densification. However, for the here investigated target materials,

the densification process in the SPS was identical. All samples reach a densification level of >95 % (**Table SI-6)** and exhibit a similar compacted microstructure (**Figure SI-10**). Additionally, the phase quality in comparison to the as-prepared powdered samples was maintained (**Figure SI-11)**. Therefore, differences in the observed characteristics can be related to the chemical modification on the *X*-site. By comparing the three investigated samples, it must be noted that the carbonitride phase $V_2GeC_{0.5}N_{0.5}$ displays electrical resistivity values between those of the parent phases, contrary to the comparable 211 carbonitride MAX phase system $Ti_2AlC_{0.5}N_{0.5}$.[34] This in turn allows to tailor the electronic transport over a significantly larger range compared to the Ti-Al-C-N system and enables a continuous monotonic tuning of electrical transport properties by *X*-site modifications related to the nitrogen content in $V_2GeC_{1-x}N_x$.

CONCLUSION

In this work we have demonstrated the MAX phase synthesis of V_2GeC, the hitherto unknown carbonitride phase with the nominal sum formula $V_2GeC_{0.5}N_{0.5}$ and the first experimental evidence for the nitride phase V_2GeN, using a hybrid solid-state preparation procedure consisting of a microwave-assisted precursor synthesis followed by a conventional heat treatment and densification by spark plasma sintering. Rietveld refinements provide the first crystallographic data for $V_2GeC_{0.5}N_{0.5}$, as well as for V_2GeN, and confirm a constant decrease in the cell volume going from carbide to nitride. SEM micrographs reveal the MAX phase-typical anisotropic morphology, which was not influenced by the composition or longer reaction times. HAXPES shows the local chemical environments, identifies secondary and surface species, and confirms the carbon to nitrogen ratio to be almost 50:50. To further elucidate their functional properties, magnetic and electrical resistivity measurements were performed. All phases exhibit paramagnetic behavior at room temperature with the potential to be specifically influenced by composition

modifications on the *X*-site of the MAX phase structure. All samples exhibit a magnetic phase transition in the temperature region of 160 K - 200 K, however, its exact nature still must be elucidated. Likewise, resistivity measurements confirm the trend of specifically influencing the functional properties of the V-Ge-C-N system by varying the composition of the *X*-site, since a higher nitrogen amount leads to a lower resistivity. All in all, these findings strongly demonstrate the demand for research in (carbo)nitride MAX phases, which can serve as new starting materials for additional solid-solution experiments. This can drive improved and targeted materials synthesis to challenge property limits (e.g. magnetism, electrical conductivity) which are hitherto predominantly dictated by carbides and their *M*-site solid-solutions.

Supporting Information. The following files are available free of charge.

PDF document including additional synthesis parameters, SEM/EDX data, X-ray diffraction data and refinement results, magnetic analysis and HAXPES data.

Corresponding Author

*christina.birkel@asu.edu

Author Contributions

The manuscript was written through contributions of all authors. All authors have given approval to the final version of the manuscript.

Funding Sources

This work has been supported by the Deutsche Forschungsgemeinschaft (DFG, German Research Foundation) within CRC/TRR 270, projects B03, B01 and A01, (Project-ID 405553726). A.A.R acknowledges the support from the Department of Chemistry, UCL. A.R. acknowledges support

from the Analytical Chemistry Trust Fund for her CAMS-UK Fellowship. A.R. acknowledges the support from the Institute of Physics (IOP) carer's fund, which provided financial support to enable her to attend the HAXPES experiments at PETRA III in person.

Acknowledgements

We acknowledge DESY (Hamburg, Germany), a member of the Helmholtz Association HGF, for the provision of experimental facilities. Parts of this research were carried out at PETRA III using beamline P22. Beamtime was allocated for proposal I-20221270.

REFERENCES

(1) Kudielka, H.; Rohde, H. Strukturuntersuchungen an Carbosulfiden von Titan Und Zirkon. *Zeitschrift für Krist.* **1960**, *114*, 447–456.

(2) Jeitschko, W.; Nowotny, H.; Benesovsky, F. Ternäre Carbide Und Nitride in Systemen: Übergangsmetall-Metametall-Kohlenstoff (Stickstoff). *Monatshefte für Chemie* **1964**, *95* (1), 156–157.

(3) Jeitschko, W.; Nowotny, H.; Benesovsky, F. Kohlenstoffhaltige Ternäre Phasen (H-Phase). *Monatshefte für Chemie* **1963**, *94*, 672–676.

(4) Jeitschko, W.; Nowotny, H.; Benesovsky, F. Die H-Phasen: Ti_2CdC, Ti_2GaC, Ti_2GaN, Ti_2InN, Zr_2InN Und Nb_2GaC. *Monatshefte für Chemie* **1964**, *95* (1), 178–179.

(5) Jeitschko, W.; Nowotny, H.; Benesovsky, F. Kohlenstoffhaltige Ternäre Verbindungen (V-Ge-C, Nb-Ga-C, Ta-Ga-C, Ta-Ge-C, Cr-Ga-C Und Cr-Ge-C). *Monatshefte für Chemie* **1963**, *94* (5), 844–850.

(6) Barsoum, M. W.; El-Raghy, T. Synthesis and Characterization of a Remarkable Ceramic: Ti_3SiC_2. *J. Am. Ceram. Soc.* **1996**, *79* (7), 1953–1956.

(7) Barsoum, M. W. The $M_{n+1}AX_n$ Phases : A New Class of Solids. *Prog. Solid State Chem.* **2000**, *28*, 201–281.

(8) Sokol, M.; Natu, V.; Kota, S.; Barsoum, M. W. On the Chemical Diversity of the MAX Phases. *Trends Chem.* **2019**, *1* (2), 210–223.

(9) Kubitza, N.; Xie, R.; Tarasov, I.; Shen, C.; Zhang, H.; Wiedwald, U.; Birkel, C. S. Microwave-Assisted Synthesis of the New Solid-Solution $(V_{1-x}Cr_x)_2GaC$ ($0 \leq x \leq 1$), a Pauli Paramagnet Almost Matching the Stoner Criterion for x = 0.80. *Chem. Mater.* **2023**, *35* (11), 4427–4434.

(10) Horlait, D.; Grasso, S.; Chroneos, A.; Lee, W. E. Attempts to Synthesise Quaternary MAX Phases $(Zr,M)_2AlC$ and $Zr_2(Al,A)C$ as a Way to Approach Zr_2AlC. *Mater. Res. Lett.* **2016**, *4* (3), 137–144.

(11) Salama, I.; El-Raghy, T.; Barsoum, M. W. Synthesis and Mechanical Properties of Nb_2AlC and $(Ti,Nb)_2AlC$. *J. Alloys Compd.* **2002**, *347* (1), 271–278.

(12) Cabioch, T.; Eklund, P.; Mauchamp, V.; Jaouen, M.; Barsoum, M. W. Tailoring of the Thermal Expansion of $Cr_2(Al_x,Ge_{1-x})C$ Phases. *J. Eur. Ceram. Soc.* **2013**, *33* (4), 897–904.

(13) Tao, Q.; Lu, J.; Dahlqvist, M.; Mockute, A.; Calder, S.; Petruhins, A.; Meshkian, R.; Rivin, O.; Potashnikov, D.; Caspi, E. N. Atomically Layered and Ordered Rare-Earth i-MAX Phases: A New Class of Magnetic Quaternary Compounds. *Chem. Mater.* **2019**, *31* (7),

2476–2485.

(14) Liu, Z.; Wu, E.; Wang, J.; Qian, Y.; Xiang, H.; Li, X.; Jin, Q.; Sun, G.; Chen, X.; Wang, J.; Li, M. Crystal Structure and Formation Mechanism of $(Cr_{2/3}Ti_{1/3})_3AlC_2$ MAX Phase. *Acta Mater.* **2014**, *73*, 186–193.

(15) Tan, Y.; Xia, Y.; Teng, Z.; Chen, C.; Zhou, X.; Zhang, H. Synthesis and Enhanced Mechanical Properties of Compositionally Complex MAX Phases. *J. Eur. Ceram. Soc.* **2021**, *41* (8), 4658–4665.

(16) Chen, L.; Li, Y.; Chen, K.; Bai, X.; Li, M.; Du, S.; Chai, Z.; Huang, Q. Synthesis and Characterization of Medium-/High-Entropy M_2SnC (M=Ti/V/Nb/Zr/Hf) MAX Phases. *Small Struct.* **2023**, *4* (1), 2200161.

(17) Du, Z.; Wu, C.; Chen, Y.; Zhu, Q.; Cui, Y.; Wang, H.; Zhang, Y.; Chen, X.; Shang, J.; Li, B.; Chen, W.; Liu, C.; Yang, S. High-Entropy Carbonitride MAX Phases and Their Derivative MXenes. *Adv. Energy Mater.* **2022**, *12* (6), 2103228.

(18) Dahlqvist, M.; Barsoum, M. W.; Rosen, J. MAX Phases – Past, Present, and Future. *Mater. Today* **2023**. https://doi.org/10.1016/J.MATTOD.2023.11.010.

(19) Kubitza, N.; Büchner, C.; Sinclair, J.; Snyder, R.; Birkel, C. S. Extending the Chemistry of Layered Solids and Nanosheets: Chemistry and Structure of MAX Phases, MAB Phases and MXenes. *Chempluschem* **2023**, *88*, e202300214.

(20) Ding, H.; Li, Y.; Li, M.; Chen, K.; Liang, K.; Chen, G.; Lu, J.; Palisaitis, J.; Persson, P. O. Å.; Eklund, P.; Hultman, L.; Du, S.; Chai, Z.; Gogotsi, Y.; Huang, Q. Chemical Scissor–

Mediated Structural Editing of Layered Transition Metal Carbides. *Science (80).* **2023**, *379* (6637), 1130–1135.

(21) Bortolozo, A. D.; Sant'Anna, O. H.; dos Santos, C. A. M.; Machado, A. J. S. Superconductivity in the Hexagonal-Layered Nanolaminates Ti_2InC Compound. *Solid State Commun.* **2007**, *144* (10–11), 419–421.

(22) Bortolozo, A. D.; Sant'Anna, O. H.; Dos Santos, C. A. M.; MacHado, A. J. S. Superconductivity at 9.5 K in the Ti_2GeC Compound. *Mater. Sci. 2012 302* **2012**, *30* (2), 92–97.

(23) Bortolozo, A. D.; Sant'Anna, O. H.; da Luz, M. S.; dos Santos, C. A. M.; Pereira, A. S.; Trentin, K. S.; Machado, A. J. S. Superconductivity in the Nb_2SnC Compound. *Solid State Commun.* **2006**, *139* (2), 57–59.

(24) Naguib, M.; Mashtalir, O.; Carle, J.; Presser, V.; Lu, J.; Hultman, L.; Gogotsi, Y.; Barsoum, M. W. Two-Dimensional Transition Metal Carbides. *ACS Nano* **2012**, *6* (2), 1322–1331.

(25) Lim, K. R. G.; Shekhirev, M.; Wyatt, B. C.; Anasori, B.; Gogotsi, Y.; Seh, Z. W. Fundamentals of MXene Synthesis. *Nat. Synth.* **2022**, *1* (8), 601–614.

(26) Siebert, J. P.; Mallett, S.; Juelsholt, M.; Pazniak, H.; Wiedwald, U.; Page De, K.; Birkel, C. S., Structure Determination and Magnetic Properties of the Mn-Doped MAX Phase Cr_2GaC.*Mater. Chem. Front* **2021**, *5*, 6082.

(27) Hamm, C. M.; Bocarsly, J. D.; Seward, G.; Kramm, U. I.; Birkel, C. S. Non-Conventional Synthesis and Magnetic Properties of MAX Phases $(Cr/Mn)_2AlC$ and $(Cr/Fe)_2AlC$. *J.*

Mater. Chem. C **2017**, *5* (23), 5700–5708.

(28) Rosen, A. S. I. and M. D. and J.; Ingason, A. S.; Dahlqvist, M.; Rosén, J.; Ingason, A. S.; Dahlqvist, M.; Rosén, J.; Max, M. Magnetic MAX Phases from Theory and Experiments; a Review. *J. Phys. Condens. Matter* **2016**, *28* (43), 433003.

(29) Hamm, C. M.; Dürrschnabel, M.; Molina-Luna, L.; Salikhov, R.; Spoddig, D.; Farle, M.; Wiedwald, U.; Birkel, C. S. Structural, Magnetic and Electrical Transport Properties of Non-Conventionally Prepared MAX Phases V_2AlC and $(V/Mn)_2AlC$. *Mater. Chem. Front.* **2018**, *2* (3), 483–490.

(30) Jeitschko, W.; Nowotny, I. L.; Benesovsky, F.; Nowotny, H.; Benesovsky, F. Die H-Phasen: Ti_2CdC, Ti_2GaC, Ti_2GaN, Ti_2InN, Zr_2InN Und Nb_2GaC. *Monatshefte für Chemie* **1964**, *95* (1), 178–179.

(31) Jeitschko, W.; Nowotny, H.; Benesovsky, F. Ti_2AlN, Eine Stickstoffhaltige H-Phase. *Monatshefte für Chemie* **1963**, *94* (6), 1198–1200.

(32) Greenaway, A. L.; Melamed, C. L.; Tellekamp, M. B.; Woods-Robinson, R.; Toberer, E. S.; Neilson, J. R.; Tamboli, A. C. Ternary Nitride Materials: Fundamentals and Emerging Device Applications. *Annu. Rev. Mater. Res.* **2020**, *51*, 1–28.

(33) Kubitza, N.; Reitz, A.; Zieschang, A.-M.; Pazniak, H.; Albert, B.; Kalha, C.; Schlueter, C.; Regoutz, A.; Wiedwald, U.; Birkel, C. S. From MAX Phase Carbides to Nitrides: Synthesis of V_2GaC, V_2GaN, and the Carbonitride $V_2GaC_{1-x}N_x$. *Inorg. Chem.* **2022**, *61* (28), 10634–10641.

(34) Scabarozi, T.; Ganguly, A.; Hettinger, J. D.; Lofland, S. E.; Amini, S.; Finkel, P.; El-Raghy, T.; Barsoum, M. W. Electronic and Thermal Properties of $Ti_3Al(C_{0.5},N_{0.5})_2$, $Ti_2Al(C_{0.5},N_{0.5})$ and Ti_2AlN. *J. Appl. Phys.* **2008**, *104* (7), 73713.

(35) Liu, Z.; Waki, T.; Tabata, Y.; Yuge, K.; Nakamura, H.; Watanabe, I. Magnetic Ground State of the $M_{n+1}AX_n$-Phase Nitride Cr_2GaN. *Phys. Rev. B - Condens. Matter Mater. Phys.* **2013**, *88* (13), 1–7.

(36) Tong, H.; Lin, S.; Huang, Y.; Tong, P.; Song, W.; Sun, Y. Difference in Physical Properties of MAX-Phase Compounds Cr_2GaC and Cr_2GaN Induced by an Anomalous Structure Change in Cr_2GaN. *Intermetallics* **2019**, *105* (November 2018), 39–43.

(37) Siebert, J. P.; Mallett, S.; Juelsholt, M.; Pazniak, H.; Wiedwald, U.; Page De, K.; Birkel, C. S.; Page, K.; Birkel, C. S. Structure Determination and Magnetic Properties of the Mn-Doped MAX Phase Cr_2GaC. *Mater. Chem. Front.* **2021**, *5* (16), 6082–6091.

(38) Lin, S.; Tong, P.; Wang, B. S.; Huang, Y. N.; Lu, W. J.; Shao, D. F.; Zhao, B. C.; Song, W. H.; Sun, Y. P. Magnetic and Electrical/Thermal Transport Properties of Mn-Doped $M_{n+1}AX_n$ Phase Compounds $Cr_{2-x}Mn_xGaC$ ($0 \leq x \leq 1$). *J. Appl. Phys.* **2013**, *113* (5), 53502.

(39) Yan, M.; Li, C.; Zou, Y.; Yang, M. Synthesis and Characterization of Magnetic MAX Phase $(Cr_{2-x}Mn_x)GaC$. *J. Wuhan Univ. Technol. Sci. Ed. 2020 352* **2020**, *35* (2), 363–367.

(40) Li, Y.; Liang, J.; Ding, H.; Lu, J.; Mu, X.; Yan, P.; Zhang, X.; Chen, K.; Li, M.; Persson, P. O. Å.; Hultman, L.; Eklund, P.; Du, S.; Yang, H.; Chai, Z.; Huang, Q. Near-Room Temperature Ferromagnetic Behavior of Single-Atom-Thick 2D Iron in Nanolaminated Ternary MAX Phases. *Appl. Phys. Rev.* **2021**, *8* (3), 31418.

(41) Yan, M.; Huang, J.; Yang, M.; Zhang, H.; Zhu, Y.; Zhou, N.; Wang, J. Synthesis and Magnetic Studies of Mn/Fe/Co Doping V_2SnC Ternary Ceramics. *Ceram. Int.* **2023**, *49* (9, Part A), 13916–13923.

(42) Manoun, B.; Amini, S.; Gupta, S.; Saxena, S. K.; Barsoum, M. W. On the Compression Behavior of Cr_2GeC and V_2GeC up to Quasi-Hydrostatic Pressures of 50 GPa. *J. Phys. Condens. Matter* **2007**, *19* (45), 456218.

(43) Magnuson, M.; Wilhelmsson, O.; Mattesini, M.; Li, S.; Ahuja, R.; Eriksson, O.; Högberg, H.; Hultman, L.; Jansson, U. Anisotropy in the Electronic Structure of V_2GeC Investigated by Soft X-Ray Emission Spectroscopy and First-Principles Theory. *Phys. Rev. B* **2008**, *78* (3), 35117.

(44) Lin, S.; Huang, Y.; Zu, L.; Kan, X.; Lin, J.; Song, W.; Tong, P.; Zhu, X.; Sun, Y. Alloying Effects on Structural, Magnetic, and Electrical/Thermal Transport Properties in MAX-Phase $Cr_{2-x}M_xGeC$ (M = Ti, V, Mn, Fe, and Mo). *J. Alloys Compd.* **2016**, *680*, 452–461.

(45) Siebert, J. P.; Patarakun, K.; Birkel, C. S. Mechanistic Insights into the Nonconventional Sol−Gel Synthesis of MAX Phase M_2GeC (M = V, Cr). *Inorg. Chem.* **2022**, *61* (3), 1603–1610.

(46) Vaidhyanathan, B.; Agrawal, D. K.; Roy, R. Novel Synthesis of Nitride Powders by Microwave-Assisted Combustion. *J. Mater. Res.* **2000**, *15* (4), 974–981.

(47) Black, D.; Mendenhall, M.; Henins, A.; Filliben, J.; Cline, J. Certification of Standard Reference Material 660c for powder diffraction. *Powder Diffr*. **2020**, *35* (1), 1-12.

(48) Yi, J.-X.; Chen, P.; Li, D.-L.; Xiao, X.-B.; Zhang, W.-B.; Tang, B.-Y. Elastic and Electronic Properties of a New MAX Compound $(Cr_{0.5}V_{0.5})_2GeC$ from First-Principles Calculations. *Solid State Commun.* **2010**, *150* (1), 49–53.

(49) Schlueter, C.; Gloskovskii, A.; Ederer, K.; Schostak, I.; Piec, S.; Sarkar, I.; Matveyev, Y.; Lömker, P.; Sing, M.; Claessen, R.; Wiemann, C.; Schneider, C. M.; Medjanik, K.; Schönhense, G.; Amann, P.; Nilsson, A.; Drube, W. The New Dedicated HAXPES Beamline P22 at PETRAIII. *AIP Conf. Proc.* **2019**, *2054* (January 2019).

(50) Karpenkov, D. Y.; Karpenkov, A. Y.; Skokov, K. P.; Radulov, I. A.; Zheleznyi, M.; Faske, T.; Gutfleisch, O. Pressure Dependence of Magnetic Properties in $La(Fe,Si)_{13}$: Multistimulus Responsiveness of Caloric Effects by Modeling and Experiment. *Phys. Rev. Appl.* **2020**, *13* (3), 34014.

(51) Hosoya, S.; Yamagishi, T.; Tokonami, M. Study of Electron State in Vanadium Nitride by Intensity Measurements of X-Ray Diffraction. *J. Phys. Soc. Japan* **1968**, *24* (2), 363–367.

(52) Phatak, N. A.; Saxena, S. K.; Fei, Y.; Hu, J. Synthesis of a New MAX Compound $(Cr_{0.5}V_{0.5})_2GeC$ and Its Compressive Behavior up to 49GPa. *J. Alloys Compd.* **2009**, *475* (1), 629–634.

(53) Rahm, M.; Hoffmann, R.; Ashcroft, N. W. Atomic and Ionic Radii of Elements 1–96. *Chem. - A Eur. J.* **2016**, *22* (41), 14625–14632.

(54) Cooper, A. S. Precise Lattice Constants of Germanium, Aluminum, Gallium Arsenide, Uranium, Sulphur, Quartz and Sapphire. *Acta Crystallogr.* **1962**, *15* (6), 578–582.

(55) Lin, S.; Tong, P.; Wang, B. S.; Huang, Y. N.; Song, W. H.; Sun, Y. P. Synthesis and Characterization of Ge–Cr-Based Intermetallic Compounds: $GeCr_3$, $GeCCr_3$, and $GeNCr_3$. *J. Alloys Compd.* **2014**, *584*, 308–314.

(56) Reitz, A.; Pazniak, H.; Shen, C.; Singh, H. K.; Jayanthi, K.; Kubitza, N.; Navrotsky, A.; Zhang, H.; Wiedwald, U.; Birkel, C. S. Cr_3GeN: A Nitride with Orthorhombic Antiperovskite Structure. *Chem. Mater.* **2022**, *34* (23), 10304–10310.

(57) Liu, Z.; Waki, T.; Tabata, Y.; Nakamura, H. Mn-Doping-Induced Itinerant-Electron Ferromagnetism in Cr_2GeC. *Phys. Rev. B* **2014**, *89* (5), 54435.

(58) Liu, Z.; Takao, K.; Waki, T.; Tabata, Y.; Nakamura, H. Electron Correlation in Pauli Paramagnetic Cr_2AlC, Cr_2GaC and Cr_2GeC. *J. Phys. Conf. Ser.* **2017**, *868* (1), 12016.

(59) Hettinger, J. D.; Lofland, S. E.; Finkel, P.; Meehan, T.; Palma, J.; Harrell, K.; Gupta, S.; Ganguly, A.; El-Raghy, T.; Barsoum, M. W. Electrical Transport, Thermal Transport, and Elastic Properties of M_2AlC (M=Ti, Cr, Nb, and V). *Phys. Rev. B* **2005**, *72* (11), 115120.

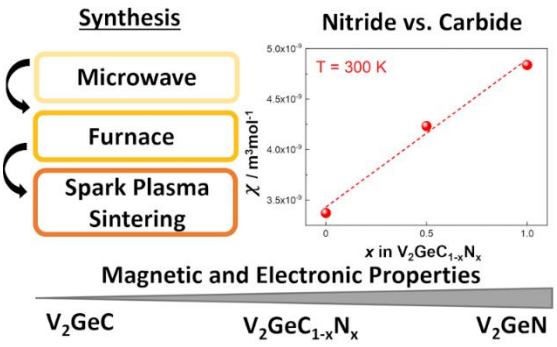
Synthesis
Microwave
Furnace
Spark Plasma Sintering
Nitride vs. Carbide
T = 300 K
χ / m³mol⁻¹
x in V2GeC1-xNx
Magnetic and Electronic Properties
V2GeC
V2GeC1-xNx
V2GeN